JOURNAL OF MATERIALS RESEARCH AND TECHNOLOGY 2023;27:1843–1856

Available online at www.sciencedirect.com

jmr&t Journal of Materials Research and Technology

journal homepage: www.elsevier.com/locate/jmrt

Review Article

Nanostructures of rare earth oxides (Ho_2O_3 and Nd_2O_3): Synthesis methods, properties, and comparative analysis

Mina Shirzadi-Ahodashti [a], *Sobhan Mortazavi-Derazkola* [b,*], *Mohammad Ali Ebrahimzadeh* [c,**]

[a] *Ramsar Campus, Mazandaran University of Medical Sciences, Ramsar, Iran*

[b] *Medical Toxicology and Drug Abuse Research Center (MTDRC), Birjand University of Medical Sciences, Birjand, Iran*

[c] *Pharmaceutical Sciences Research Center, Hemoglobinopathy Institute, School of Pharmacy, Mazandaran University of Medical Sciences, Sari, Iran*

ARTICLE INFO

Article history:
Received 1 July 2023
Accepted 8 October 2023
Available online 11 October 2023

Keywords:
Holmium oxide
Neodymium oxide
Nanostructure
Rare earth oxide

ABSTRACT

Nanostructures composed of rare earth oxides, specifically Ho_2O_3 and Nd_2O_3, exhibit a range of desirable characteristics. Notably, neodymium oxides are renowned for their distinctive electrical and optical properties. Consequently, the development of rare earth oxide nanostructures, encompassing the aforementioned compositions, has emerged as a prominent area of research. The introductory section provides an overview of recent advancements pertaining to diverse applications of these nanostructures. Due to the technological significance of this class of materials, various methods for synthesizing these rare earth oxides have been introduced. This review provides a comprehensive description and examination of the synthesis of Ho_2O_3 and Nd_2O_3 nanostructures through different techniques. Finally, a comparative analysis is conducted, considering aspects such as methodology, efficiency, morphology, and grain size of the resulting samples.

1. Introduction

In recent years, oxide materials have found extensive applications in various fields, including environmental and biomedical sciences [1]. Among these oxide materials, the rare earth oxide family has garnered significant attention from researchers due to their diverse applications in areas such as sensing, sensing, optics, etc. [1,2] (Fig. 1). These compounds are represented by the chemical formula M_2O_3. While previous review articles have explored the properties and applications of these nano oxide materials, this review aims to provide a fresh perspective on the different effects of these

* Corresponding author.
** Corresponding author.
E-mail addresses: S.mortazavi23@yahoo.com, Sobhan.mortazavi@bums.ac.ir (S. Mortazavi-Derazkola), Zadeh20@gmail.com (M.A. Ebrahimzadeh).

https://doi.org/10.1016/j.jmrt.2023.10.079

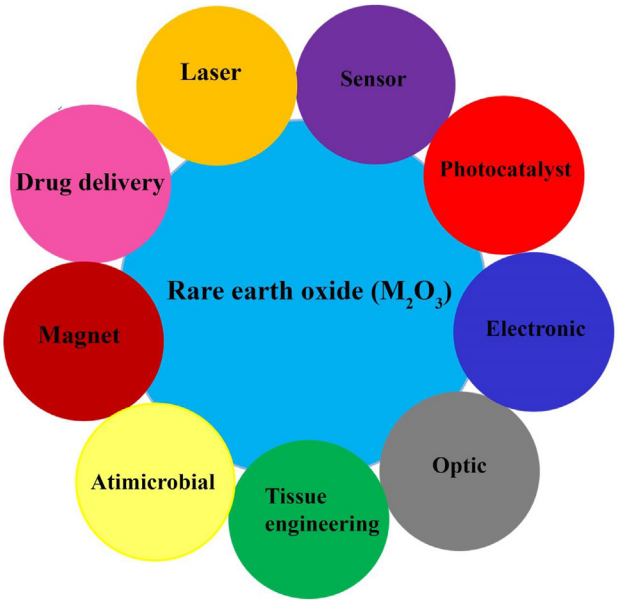

Fig. 1 – Schematic representation showing an overview of the applications of rare earth metal oxides.

materials on enhancing their performance in various applications. Research has shown that the efficiency and activity of nano materials are highly dependent on their morphology and size. Nano materials with more regular structures and optimized sizes tend to exhibit superior performance in various applications. Therefore, paying close attention to the morphological aspects and sizes of nano materials is of paramount importance. Over the past two decades, significant advancements have been achieved in the design and synthesis of rare earth (RE) oxides, enabling precise control over size and various morphologies [3,4]. Rare earth oxides play a pivotal role across various research domains and scientific realms, including ceramic industries [5], catalysis, sensors, optics and magnetics (5) [6], as well as electronics, energy conversion, and chemical reactivity [3]. Moreover, these compounds hold considerable promise in medical and biochemical systems [7], and are fundamental constituents of solid electrolytes, finding widespread use as additives to enhance ion conductivity [8]. Notably, among these nanomaterials, rare earth metal oxides such as Ho_2O_3 and Nd_2O_3 exhibit exceptional optical and electrical properties, rendering them particularly captivating and promising.

In this section, we delve into the nanostructures of Ho_2O_3 and Nd_2O_3, exploring their respective applications. Holmium oxide (Ho_2O_3) has garnered extensive attention owing to its unique and exceptional utility in wavelength-calibration instruments, pyrolysis catalysts, and its high potential for application as a contrast agent in magnetic resonance imaging (MRI) [9,10]. A compilation of recent literature elucidating the manifold uses of Ho_2O_3 and Nd_2O_3 is presented in Table 1 and Table 2. Due to the light-stimulated degradation of atmospheric pollutants, aqueous contaminants, and organic pollutants, photocatalysis has attracted more attention lately [11]. In fact, photocatalytic technology stands out as a cost-effective and straightforward method for the elimination of both organic and inorganic pollutants [12]. Ln_2O_3 nanostructures have found application in photocatalysis. Mortazavi-Derazkola and Zinatloo-Ajabshir have conducted investigations into the photocatalytic degradation potential of Ho_2O_3 nanostructures [13,14]. Mortazavi-Derazkola et al. demonstrated that Ho_2O_3 nanostructures, when employed as a photocatalyst, led to a significant degradation of eriochrome black T dye upon minimal exposure to UV light radiation. In a parallel study, Zinatloo-Ajabshir et al. investigated the impact of various capping agents on the morphology, size, and photocatalytic performance of Ho_2O_3. The outcomes highlighted the substantial influence of capping agent selection on the size, shape, and control of photocatalytic behavior. For the treatment of diverse cancer types, utilizing radionuclide therapy with nano-sized carriers has emerged as a promising approach. Kim et al. revealed that holmium (^{165}Ho), distinguished by its abundant natural isotopic composition of 100 % and a substantial thermal neutron capture cross-section leading to activation to ^{166}Ho, was identified as a 'theranostic' agent [15]. Kim's investigations further demonstrated that Mesoporous Carbon Nanoparticles (MCNs) containing non-radioactive holmium exhibited no cytotoxicity in vitro studies (using human ovarian cancer cells), underscoring their suitability as non-radioactive therapeutic agents for diverse cancer treatments. Magneto-optical materials (MOE), encompassing crystal, glasses, and ceramic, play a pivotal role in applications such as optical fiber sensors, optical isolators, and Faraday rotator modulators [16]. Among these materials, the high-optical-quality magneto-optical ceramic have emerged as promising alternatives to single crystals and glasses, due to attributes such as high thermal conductivity, thermostability, near-net shaping capabilities, resistance to heat shocks, larger sizes, and ease of mass production [17,18]. In the pursuit of minimizing heat generation resulting from the absorption of magneto-optical materials in kilowatt laser systems, the development of novel functional MOEs with low absorption coefficients and high Verdet constants becomes crucial. The substantial concentration of rare-earth cations, such as Ho3+, Dy3+, and Tb3+, in their sesquioxides contributes to a greater Verdet constant compared to garnet structures [19].

In 2017, Furse et al. reported a groundbreaking discovery that holmium oxide (Ho_2O_3) ceramics possess the potential to serve in high-average-power lasers [20]. Transparent magneto-optical Ho_2O_3 ceramics were subsequently fabricated by Cheng and Lu through vacuum sintering. Cheng employed self-reactive resultant HoOF as a sintering aid, while Lu utilized sulfate-exchanged nitrate-type layered rare-earth hydroxide as a precipitation precursor [21,22]. Magneto-optical Ho_2O_3 ceramics produced by Cheng et al. exhibited a Verdet constant of -182 ± 8, -46 ± 3, and -22 ± 2 rad/Tm at 633 nm, 1064 nm, and 1550 nm, respectively. These ceramics also demonstrated an in-line transmittance of 72.0 % at a wavelength of 1550 nm. In a similar vein, Lu et al. prepared a magneto-optical Ho2O3 ceramic featuring a Verdet constant of −180, −46, and −20 rad/Tm at 632 nm, 1064 nm, and 1550 nm. Notably, this ceramic exhibited an in-line transmittance of approximately 73 % at a wavelength of 1000 nm. Their results collectively suggest that Holmium oxide ceramics hold substantial promise for application within high-power infrared laser systems. Guo's studies marked another significant milestone as Ho_2O_3 nanomaterials were harnessed for humidity detection for the first time. Impressively, these

Table 1 – Different applications of synthesized holmium oxide and neodymium oxide nanoparticles by different methods along with the details of their synthetic parameters.

Sample	Application	Method	Size (nm)	Morphology	Temp.	Ref
Ho_2O_3	Radiotherapeutic	Wet-impregnation	154	Spherical	–	[15]
Ho_2O_3	Paramagnetic	Hydrothermal	50-200 500 130	Nanowires Nanosheet Nanoplate	900(°C)	[9]
Ho_2O_3	Transparent magneto-optical	Vacuum sintering	90	Spherical	1400(°C)	[21]
Ho_2O_3	Transparent magneto-optical	Precipitation	47	Spherical	1050(°C)	[22]
Ho_2O_3	Transparent magneto-optical	Pulse electric current sintering	350	Spherical	1100(°C)	[20]
Nd_2O_3	Gas sensing	Co-precipitation	700	–	600(°C)	[37]
Nd_2O_3	Optical properties	Thermal decompose	35 ± 6 nm 46 ± 4 nm	–	500(°C) 800(°C)	[55]

Table 2 – Photocatalytic application of synthesized holmium oxide and neodymium oxide nanoparticles by different methods along with the details of their synthetic parameters.

Sample	Pollutant	Method	Precipitator	Capping agent	Morphology	Size (nm)	Temp.	Ref
Ho_2O_3	Eriochrome black T	Hydrothermal	Tepa	Schiff base[a]	Spherical	12–35	600(°C)	[13]
Ho_2O_3	Erythrosine	Sonochemical	Dien	Schiff base[b] Oleylamine PVA	Spherical Sphere-like Spherical	14–54	–	[25]
Nd_2O_3	Methylene blue	Precipitation	Triethylenetetramine	Schiff base[c] Titriplex SDBS	Non uniform Non uniform Spherical	10–40	700(°C)	[32]
Nd_2O_3	Eriochrome black T	Hydrothermal	Tepa	Schiff base[a]	Rod	26	700(°C)	[33]
Nd_2O_3	Eosin Y	Sonochemical	2,2-dimethyl-1, 3-propanediamine	Schiff base[d] Titriplex PVP	Non uniform Non uniform Spherical	15–75	650(°C)	[39]

Tepa: tetraethylenepentamine.
Dien: diethylenetriamine.
PVA[a]: polyvinyl alcohol PVP[b]: Polyvinylpyrrolidone.
Schiff base[a]: bis-(2-hydroxy-1-naphthaldehyde)-o-phenylenediamine.
Schiff base [b]: bis-(2- hydroxy-1-naphthaldehyde)-4,4'-diaminodiphenylmethan.
Schiff base[c:] bis-(2-hydroxy-1- naphthaldehyde)-propandiamine.
Schiff base[d]: bis-(2- hydroxy-1-naphthaldehyde)-4,4'-methylenedianiline.

nanomaterials exhibited exceptional capabilities in humidity sensing, spanning from fingertip and body surface humidity to respiratory sensing. These attributes underscore their potential in various domains such as human vital sign monitoring, human activity detection, and moisturizing effectiveness assessments [23]. Recent years have witnessed the emergence of multiple methodologies for Ho_2O_3 synthesis. Diverse techniques have been introduced to attain Ho_2O_3 with tailored properties, encompassing the hydrothermal method [9], thermal decomposition [24], sonochemical processes [25], electrochemical deposition [26], pulse electric current sintering technique [19], precipitation [14], and vacuum sintering [21].

Conversely, neodymium oxide has gained significant attention due to its potential applications in recent years. Following cerium and lanthanum, neodymium stands as one of the most abundant rare earth elements. Characterized by hexagonal crystals, Nd_2O_3, a light grayish-blue compound, finds utility in the synthesis of solid-state lasers. The dichroic nature of Nd_2O_3 has led to its incorporation in the production of sunglasses, welding goggles, and other glass-based materials. Among the array of rare earth oxides, neodymium oxide (Nd_2O_3) has garnered notable recognition owing to its distinct electrical and optical attributes. Its diverse applications encompass enhancing luminescent materials, serving as a catalyst in the automotive industry, functioning as a glass-polishing agent, UV absorbent, photonic material, gas sensor, protective coating, and contributing to lung cancer treatment. These multifarious usages have sparked heightened interest in the fabrication of nanocrystalline Nd_2O_3 [3,27,28]. Barbora et al. introduced composite membranes of synthesized Nd_2O_3/nafion with potential utility in direct alcohol fuel cells. The Nd_2O_3/nafion composite membrane exhibited superior ion exchange capacity, tensile strength, proton conductivity, oxidation stability, and water uptake compared to the pure cast nafion membrane. Consequently, its application in fuel cells becomes feasible [8]. Through the synthesis of a 1:1 (w/w) electrode composite of graphite and Nd_2O_3 nanoparticle grafted graphene (NOGG), Biswasa et al. demonstrated the potential of the GP/NOGG electrode. This electrode showcased remarkable sensitivity, selectivity, and reproducibility. It emerges as a promising electrochemical sensor for the detection and analysis of Adrenaline (AD) and Tyrosine (TY) in pharmaceutical and biological samples, displaying excellent recovery rates. The GP/NOGG electrode holds promise for future clinical diagnoses of AD and TY [29].

Al-Fakeh et al.'s research revealed that a complex containing Nd_2O_3 nanoparticles exhibits antioxidant and antibacterial properties against *Staphylococcus aureus* and *Salmonella typhimurium* strains. Consequently, this study opens new avenues for exploration in biomedical applications [30]. In recent years, considerable emphasis has been placed on the exploration of environmentally friendly catalysts. Nanoparticles characterized by their substantial specific surfaces, minute particle dimensions, and pronounced chemical reactivity, have rich role in catalyst research. Yang et al. conducted an investigation into the catalytic prowess of nanoscale Nd_2O_3 in the synthesis of isobutyl acetate [31]. Their findings underscored the potential for a multitude of nanopowders to be harnessed in various applications, ranging from environmentally benign catalysts to ceramic materials, thereby optimizing resource utilization and expediting processes. The work by Yang further illuminated a direct correlation between diminished particle size and heightened catalytic activity. Zinatloo-Ajabshir and Mortazavi-Derazkola delved into the realm of Nd_2O_3 nanostructures, crafting and evaluating their photocatalytic efficacy in the degradation of pollutants. Their studies encompassed the removal of methylene blue [32], eriochrome black T dye [33], and methyl orange (MO) from water [7], signifying the multifaceted potential of these nanostructures in addressing environmental challenges. Zinatloo-Ajabshir et al. highlighted the paramount significance of parameters such as particle size, shape, and pore distribution in neodymium oxide for governing its photocatalytic performance. Mortazavi-Derazkola et al. demonstrated that Nd_2O_3 nanoparticles have a good capability for the removal of methyl orange (MO) and probably other organic pollutants from aqueous environments. Huang [4] and Mortazavi-Derazkola [27] further contributed to this area by investigating the impact of surfactant type and concentration on the morphology and particle size of Nd_2O_3. The findings of Huang were substantiated by Mortazavi-Derazkola, collectively affirming the influential role of surfactants in shaping neodymium oxide's morphology and particle dimensions.

Numerous methods have been documented for the synthesis of Nd_2O_3, encompassing diverse approaches such as radiofrequency thermal plasma route [34], hydrothermal method [35], HPMR method [6], microwave irradiation (MWI) [36], thermal decomposition [5], coprecipitation method [37], solution combustion [28], green synthesis [38], precipitation method [32], sonochemical process [39], sol-gel process [40], and inverse microemulsion technique [41]. In this review, we delve into an exploration of various synthesis methods aimed at enhancing the efficiency and efficacy of these compounds across a spectrum of applications. The objectives of this review encompass the following key points: (i) Investigation of various synthesis methods for nanoscale holmium oxide structures. (ii) Examination of different synthesis techniques for nanoscale neodymium oxide structures. (iii) Comparative analysis of the morphology and size of nanoscale holmium oxide structures synthesized through different methods. (iv) Comparative analysis of the morphology and size of nanoscale neodymium oxide structures synthesized through different methods. (v) Concluding the optimal synthesis approach for neodymium oxide and holmium oxide nanoscale structures. (vi) Through a comprehensive examination of these objectives, this review aims to shed light on the diverse synthesis techniques available for rare earth oxide nanostructures, enabling researchers and scientists to make informed decisions in choosing the most suitable methods for their specific applications.

2. Methods for preparing Ho_2O_3 and Nd_2O_3 nanostructures

The synthesis technique characterizes the applications and properties of material, which depend on their compositions, morphology, and phase structures. The approaches utilized for the fabrication of rare earth oxides (Ln_2O_3, Ln = Ho, Nd) are elucidated in this review (Fig. 2). The previously mentioned methods for synthesizing rare earth holmium oxide and neodymium oxide are detailed in the subsequent section.

2.1. *Hydrothermal*

Hydrothermal synthesis stands as one of the most frequently employed techniques for the preparation of nanostructures. This method appears highly promising due to its convenience and simplicity, enabling the controlled production of well-defined crystalline structures by regulating parameters such as time, pH, and temperature [42,43]. Therefore, in this review, we examine the synthesis of holmium oxide nanostructures using the hydrothermal method and the obtained results of this composition. Mortazavi-Derazkola et al. accomplished the production of pristine Ho_2O_3 nanostructures through the thermal conversion of $Ho(OH)_3$ nanostructures in an air environment at 600 °C for a duration of 4 h [13]. The $Ho(OH)_3$ nanostructures were synthesized utilizing the hydrothermal approach. They investigated the effect of different factors on

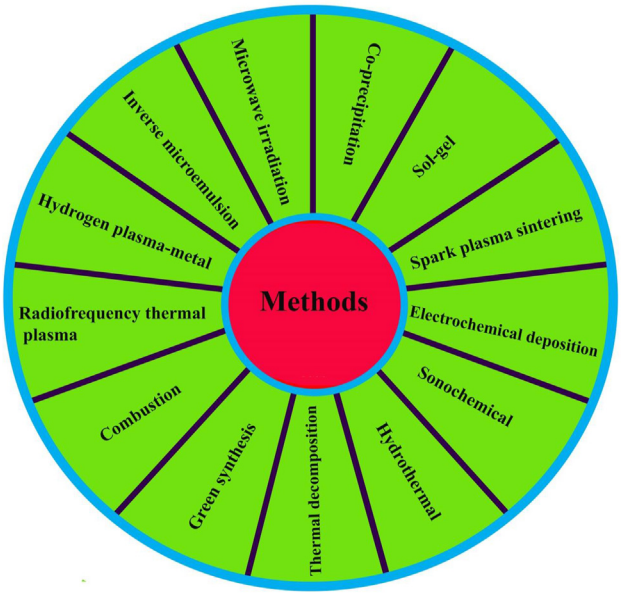

Fig. 2 – Schematic representation showing the synthesis methods of holmium oxide and neodymium oxide of this review article.

the morphology and size of the final product, such as capping agent (bis-(2-hydroxy-1-naphthaldehyde)-o- phenylenediamine Schiff base ligand), temperature (120, 160, 200 °C), precipitator (NH_3, tetraethylenepentamine), and time (12, 16, 20 h). The results of FESEM and TEM analyses showed that the most optimal combination of holmium hydroxide was obtained under the conditions of 12 h of reaction, a temperature of 160 °C, using tetraethylenepentamine as a precipitant, and in the presence of a Schiff base compound. Spherical morphology and regular structures were the characteristics of the optimal composition. FESEM results showed that when NH_3 precipitating agent was used, particle-like structures with high aggregation were obtained. On the other hand, tetraethylenepentamine had steric hindrance influence, which played a very important role in controlling the shape and size by preventing the accumulation of holmium hydroxide nanoparticles. Finally, through the calcination of $Ho(OH)_3$ nanostructures at 600 °C for 4 h, Ho_2O_3 nanostructures with a size of approximately 12–35 nm were successfully synthesized.

In a separate investigation, Lee et al. employed the hydrothermal method to synthesize paramagnetic Ho_2O_3 nanostructures by utilizing an aqueous solution of holmium(III) chloride hexahydrate and ammonia solution under autoclave conditions [9]. At first, they synthesized three different morphologies (nanowires, nano-square sheets, and nanoplates) of Ho_2O_3 and then investigated their physicochemical properties, including magnetism. They used different methods to synthesize three samples (wires, sheets, and plates). X-ray Diffraction (XRD) outcomes revealed that upon thermal annealing at 450 °C, all three samples exhibited broad XRD peaks located at similar positions. Specifically, the XRD patterns of nanowires and nano-square sheets bore a resemblance to each other, albeit the pattern of the nanoplates displayed slight differences. Subsequent to thermal annealing at 900 °C, all three samples showcased congruent XRD patterns characteristic of the cubic Ho_2O_3 crystal phase. Thermogravimetric analysis underscored that nanowires and nano-square sheets underwent two distinct weight loss stages, while the nanoplates exhibited three discernible stages of weight loss. The weight loss observed at 805 °C for the nanoplates was ascribed to the elimination of H_2O. These findings were confirmed by Fourier Transform Infrared (FT-IR) spectra. Notably, the FT-IR spectrum of the nanoplates retained the presence of OH groups subsequent to annealing at 450 °C; however, these groups disappeared after annealing at 900 °C. Scanning Electron Microscopy (SEM) results revealed that the morphologies of nanowires, nanosheets, and nanoplates were comparable prior to thermal treatment. Nevertheless, after exposure to thermal treatment at 900 °C, these morphologies exhibited slight shrinkage and distortion. This phenomenon was attributed to processes of dehydration/decomplexation and crystal stage transformations that transpire during thermal treatment. In general, in their research, three different morphologies of holmium oxide nanostructures were synthesized. After investigating the magnetic properties of these compounds, it was found that Ho_2O_3 nanowires, nanosquare sheets, and nanoplates had paramagnetic behaviors. They concluded that the magnetic and physicochemical properties of these compounds were completely dependent on the morphology. Jeon et al. synthesized Nd_2O_3 with a nanorods structure using the hydrothermal method [44]. To prepare $Nd(OH)_3$ nanorods, they created a mixed solution of $Nd(OH)_3$ and Nd(III) nitrate hexahydrate, utilizing an appropriate amount of the solution. Subsequently, 30 % ammonia solution was introduced to the mixed solution to induce precipitate formation. The reaction samples were designated as follows: sample A (20 mL + 5 mL H_2O + 1.0 mL NH_4OH), B (20 mL + 15 mL H_2O + 2.0 mL NH_4OH), C (20 mL + 15 mL H_2O + 0.5 mL NH_4OH), D (20 mL + 15 mL H_2O + 0.5 mL NH_4OH + 0.5 mL 30 % H_2O_2), and E (B solution at 200 °C). The resulting mixture was transferred to an autoclave and maintained in an oven at 120 °C for 12 h. Subsequent to cooling to room temperature, the white powder was subjected to centrifugation and annealed at 350 °C and 900 °C for the synthesis of NdOOH and hexagonal-phase Nd_2O_3, respectively. The SEM results exhibited that an increase in pH values and reaction temperatures led to a decrease in the aspect ratio. The width and length of the as-prepared sample exhibited increments upon the addition of H_2O_2 to the solution. Upon annealing at 700 °C, the rod-like morphology persisted, although the rods became narrower and shorter due to dehydration. At an annealing temperature of 900 °C, the rod-like morphology disappeared. To elucidate the crystal structures of the as-prepared and thermally annealed samples (350, 700, and 900 °C), X-ray diffraction crystallography was conducted. The XRD patterns after thermal treatment at 350 °C displayed distinct differences, attributed to NdOOH. Subsequent thermal annealing at 700 °C resulted in the emergence of new XRD peaks that surpassed the intensity of the NdOOH peaks. Subsequent thermal annealing at 700 °C resulted in the emergence of new XRD peaks that surpassed the intensity of the NdOOH peaks. Upon annealing at 900 °C, the crystalline phase of NdOOH vanished, and the hexagonal phase of Nd_2O_3 became predominant, corresponding to the newly emerged XRD peaks. Based on the XRD results, it can be inferred that as the annealing temperature increased, $Nd(OH)_3$ transformed successively into NdOOH and then into Nd_2O_3. The TEM analysis revealed a drastic alteration in the morphology of the Nd_2O_3 sample annealed at 900 °C, accompanied by a substantial enhancement in crystallinity. Ultimately, their research demonstrates that the hydrothermal method can produce nanorods ranging in diameter from 30 to 70 nm for $Nd(OH)_3$, with lattice spacings of 0.324 nm, and lattice distances of 0.337 nm for neodymium oxide nanoparticles.

In another study, Umesh et al. fabricated nanocrystalline Nd_2O_3 phosphors exhibiting a rod-like structure via the hydrothermal method, utilizing Nd(III) nitrate, HNO_3, and aqueous NaOH as initial materials, all under conditions of 200 °C and a duration of 24 h [28]. They successfully synthesized neodymium oxide nanoparticles using both hydrothermal and combustion techniques, followed by an investigation into their structural and optical characteristics. The selected area electron diffraction patterns (SAED) of the products exhibited a high degree of crystallinity. The result of XRD confirmed the formation of a hexagonal structure of Nd_2O_3 at a calcination temperature of 900 °C for 3 h. Furthermore, the findings indicated that the particles produced through the combustion method were predominantly spherical and

exhibited a size range from 20 to 100 nm. In contrast, the hydrothermal synthesis of Nd_2O_3 resulted in dumbbell-shaped nanorods with pointed tips and open ends, with particle sizes ranging from 25 to 90 nm. The energy band gaps of both samples were examined, revealing optical energy band gaps of 5.66 eV for the combustion method and 5.33 eV for the hydrothermal method. Consequently, it was observed that the combustion method led to an increased optical bandgap in neodymium oxide compared to the hydrothermal method. In conclusion, the low-temperature combustion route emerged as a safe, straightforward, and rapid method for producing fine and uniform Nd_2O_3 powders when compared to the alternative synthesis method.

In another study, Kepinski et al. synthesized $Nd(OH)_3$ at 180 °C using a hydrothermal methodology. Subsequent calcination at 500 °C induced the conversion of $Nd(OH)_3$ into cubic Nd_2O_3, exhibiting diverse morphologies [45]. The stability of Nd_2O_3 persisted up to 800 °C. The researchers explored the properties of precursors and their thermal transformation into neodymium oxide using a comprehensive array of techniques including XRD, TEM, HRTEM, TG, DTA, EGA-MS, FTIR, and AFM. Kepinski also underscored the pivotal role played by reaction conditions (pressure, temperature) in shaping the structure and morphology of the resulting products. The study demonstrated that the type of neodymium precursor exerted a decisive influence on the crystal structure (cubic or hexagonal) and the morphology of the neodymium oxide.

Zinatloo-Ajabshir et al. synthesized Nd_2O_3 nanostructures using the hydrothermal approach, involving the thermal conversion of nanostructured $Nd(OH)_3$ in ambient air at 700 °C for a duration of 4 h [33]. The authors explored the effects of reaction time (10, 14, and 18 h), Schiff base ligand (bis-(2-hydroxynaphthaldehyde)-1,2-phenylenediamine), and precipitator type (NH_3, ethylenediemine, triethylenetetramine, and tetraethylenepentamine) on the morphology and particle sizes of Nd_2O_3 using SEM technique. In their study, they investigated how the choice of precipitating agent affects the grain size and shape of both neodymium hydroxide and neodymium oxide. The results obtained through SEM analysis revealed that ammonia, ethylenediamine, triethylenetetramine, and tetraethylenepentamine led to the formation of irregular micro/nanostructures, irregular spherical nanopackets, irregular nanorods/non-uniform spherical nanoparticles, and relatively uniform nanorods, respectively. Changing the type of precipitant resulted in a reduction in grain size due to an increase in the spatial barrier effect. With a greater steric hindrance influence, there was less accumulation of nano-essence, and nucleation occurred instead of particle growth. Consequently, the most effective precipitating agent in their research turned out to be tetraethylenepentamine. Additional conditions were examined, leading to the conclusion that the most favorable size and morphology were achieved in the presence of a Schiff base ligand as a capping agent over a 14-h period. In the FT-IR spectrum of the nanostructured Nd_2O_3 sample, stretching vibration corresponding to (OH) groups appeared at 3425 cm^{-1}, which was attributable to the (OH) stretching vibration of the physisorbed water molecules. Notably, the distinctive peak of Nd_2O_3 appears at 500 cm^{-1}. The XRD pattern and energy-dispersive X-ray spectroscopy (EDAX) results confirmed the formation of pure Nd_2O_3 nanoparticles at the temperature of 700 °C. The particle size of the synthesized $N_{d2}O_3$ nanoparticles, determined via TEM analysis, fell within the range of 22–40 nm. The schematic diagram of rare earth metal oxide nanostructures is shown in Fig. 3.

2.2. *Thermal decomposition*

Thermal decomposition, also known as thermolysis, refers to the chemical breakdown of a substance due to the application

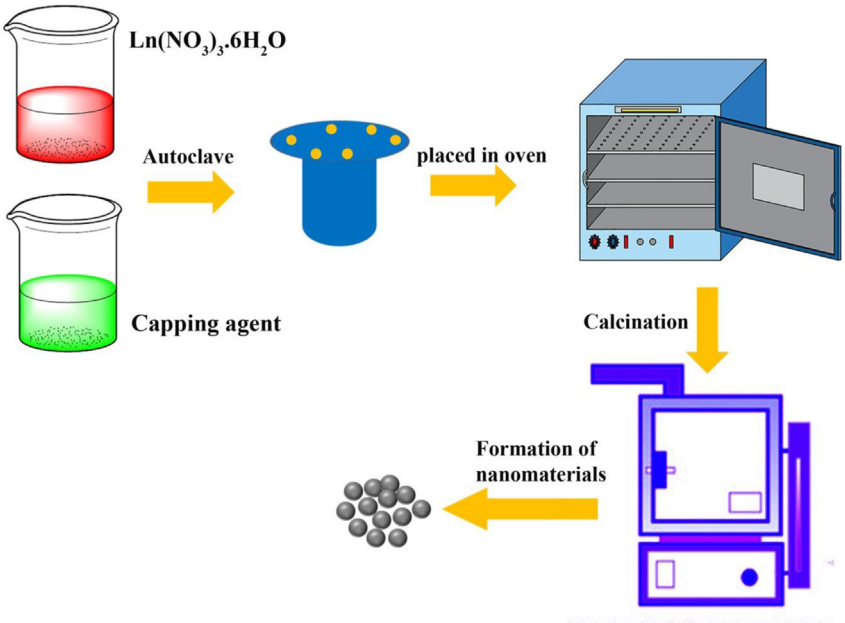

Fig. 3 – Schematic representation of the synthesis of holmium oxide and neodymium oxide using the hydrothermal method.

of heat. The decomposition temperature of a substance is the specific temperature at which the substance undergoes chemically decomposes. Abdusalyamova et al. synthesized nanocrystalline powders of holmium oxide by two methods. Holmium oxide were synthesized using acetate route and carbamide route. They synthesized holmium oxide nanocrystalline particles, ranging in size from 6 to 16 nm, using various precursors (holmium chloride, holmium acetate, and a holmium complex containing carbamide) at temperatures of 600 and 700 °C [24]. The authors further reported various observations that were contingent upon the crystallite size effect on the lattice parameter of holmium oxide. Through the utilization of XRD patterns and Raman spectroscopy, it was demonstrated that the bcc lattice parameter of the holmium oxide nanocrystalline materials surpassed that of the well-crystallized powder. Additionally, transmission electron microscopy (TEM) images revealed distinct differences in the structure and morphology of holmium oxide particles obtained from holmium chloride in comparison to those synthesized from carbamide and acetate precursors.

In a separate investigation, Mortazavi-Derazkola conducted the synthesis of holmium oxide ceramic nanostructures through the thermal decomposition method, carried out at 600 °C for 5 h [10]. This study presented the pioneering achievement of holmium oxide ceramic nanostructures synthesis, achieved by employing diverse molar ratios of holmium nitrate and bis-(2-hydroxy-1-naphthaldehyde)-butane diamine as Schiff base ligand, in a facile solvent-free reaction. EDAX pattern and XRD results established the successful formation of pure Ho_2O_3 nanoparticles at the temperature of 600 °C. The investigation encompassed a comprehensive exploration of the impact of calcination temperatures at 500, 600, and 700 °C, as well as varying molar ratios of the Schiff base ligand (L) (ranging from 1:0.5 to 1:4), on the dimensions and shapes of the holmium oxide nanoparticles. Examination of the influence of calcination temperature on nanoparticles formation showed that a temperature of 500 °C proved insufficient for precursor decomposition and subsequent nanoparticle generation. On the other hand, as temperatures escalated to 700 °C, both nanoparticle size and the extent of aggregation exhibited an increase. Consequently, a calcination temperature of 600 °C was identified as the optimal condition for nanoparticle formation. The SEM results indicated that elevating the Schiff base ligand (L) content led to nucleation dominance instead of particle growth, attributed to the steric hindrance effects of (L). Without the presence of the Schiff base ligand, the SEM images showed nanoparticles with a bulk-like structure. This observation suggests that significant ligands, as opposed to conventional capping agents, play a pivotal role in regulating particle size and morphology. The results of this research demonstrated that the molar ratio of holmium nitrate and Schiff base ligand and calcination temperature had a significant effect on the particle size and morphology of the holmium oxide in the range between 20 and 40 nm. Nd_2O_3 nanostructures were synthesized by Mortazavi-Derazkola et al. utilizing a thermal decomposition method. The novel precursor $[NdL(NO_3)_2]NO_3$, where L corresponds to bis-(2-hydroxy-1-naphthaldehyde)-ethanediamine Schiff base compound, was employed in conjunction with sodium dodecyl sulfate (SDS) as a shape- and size-controlling agent [27]. In this study, the researchers investigated the effects of SDS on the morphology and size of synthesized neodymium oxide. The morphological and optical properties of the obtained nanostructured were characterized using various techniques including TGA, XRD, EDAX, UV–Vis, FESEM, TEM, and FTIR. In the FTIR spectrum characteristic bands of the Nd_2O_3 were observed at 619 and 512 cm^{-1}. XRD results revealed that at calcination temperatures of 700 and 800 °C, pure hexagonal Nd_2O_3 did not form. However, with an increase in temperature up to 900 °C, pure hexagonal Nd_2O_3 was achieved. The purity and chemical composition of the as-synthesized nanostructured Nd_2O_3 were confirmed with the EDAX technique, which indicated the presence of Nd and O elements, thereby confirming the formation of neodymium oxide nanostructures. The optimization of different molar ratios of SDS:NdP demonstrated a significant impact on the morphology and particle size control of the Nd_2O_3. TEM images revealed that the as-synthesized Nd_2O_3 nanoparticles exhibited diameters in the range of 20–55 nm. To investigate the influence of the neodymium source and SDS on the shape of Nd_2O_3, two samples were synthesized: one utilizing $Nd(NO_3)_3{\cdot}6H_2O$ in the presence of SDS, and the other employing $NdL(NO_3)_2]NO_3$ without SDS. SEM imaging indicated that in the absence of $[NdL(NO_3)_2]NO_3$ and SDS, the structures exhibited bulk characteristics and formed highly agglomerated particle-like structures. In conclusion, the research team determined that the application of $[NdL(NO_3)_2]NO_3$ in conjunction with SDS led to the formation of Nd_2O_3 nanostructure.

In another study, Mortazavi-Derazkola et al. conducted a re-synthesis of Nd_2O_3 nanostructures using the thermal decomposition method [46]. The investigation aimed to assess the impact of calcination temperature, different molar ratios of neodymium nitrate as a precursor, and Schiff base ligand as a precipitant on the shape and particle size of the resulting Nd_2O_3. The FT-IR spectra of Schiff base ligand (L), Nd(III) complex, and Nd_2O_3 nanoparticles were taken. In the FT-IR spectra, the peaks placed at 3423 cm^{-1}, 1634 cm^{-1}, and 504 cm^{-1} were attributed to (OH) stretching, (OH) bending vibrations, and the characteristic peak of Nd_2O_3, respectively. The presence of physisorbed water molecules related to the Nd_2O_3 sample was indicated by the (OH) peak. XRD analysis of Nd_2O_3 was performed at 700, 800, and 900 °C for 5 h. The outcomes demonstrated that at 700 and 800 °C, the synthesis of pure hexagonal Nd_2O_3 did not occur; however, with an increase in calcination temperature to 900 °C, the formation of pure hexagonal neodymium structure was achieved. The assessment of purity and composition of the Nd_2O_3 product was accomplished through EDAX spectrum analysis, which confirmed the presence of Nd and O elements. Consequently, XRD and EDAX results verified the successful fabrication of cubic hexagonal Nd_2O_3 nanostructures via the thermal decomposition route. SEM images were captured for Nd(III) complexes calcined at varying calcination temperature and molar ratios of (L) Schiff base. Investigation into the effect of calcination temperature on the shape and particle size of neodymium oxide nanoparticles revealed that temperatures of 500, 600, and 700 °C were insufficient for precursor complex decomposition and subsequent nanoparticle formation. As the calcination temperature reached 800 °C, agglomerated

nanoparticles were formed. Further temperature increase to 900 °C resulted in larger particle sizes and aggregate quantities. Increasing the molar ratio of $Nd(NO_3)_3 \cdot 6H_2O$ to Schiff base ligand (L) to 1:4 led to the formation of uniform mulberry-like nanostructures. The steric hindrance effect of (L) was observed, as higher (L) correlated with reduced aggregation between Nd_2O_3 nanoparticles. To investigate the influence of (L) Schiff base ligand on the shape, one sample was synthesized without using (L) at 900 °C, resulting in the formation of bulk structures. So, the results of this research showed that the treatment temperature and the molar ratio of $Nd(NO_3)_3 \cdot 6H_2O$ to (L) have a significant impact on the morphology and particle size of Nd_2O_3. Consequently, a calcination temperature at 900 °C and a molar ratio of 1: 4 were selected as optimal conditions for synthesizing the Nd_2O_3 nanostructure. TEM images of the nanostructured Nd_2O_3 with a 1:4 M ratio [$Nd(NO_3)_3 \cdot 6H_2O$ to (L)] and calcination at 900 °C revealed quasi-spherical structures with particle sizes ranging from 20 to 50 nm.

In another study, Phuruangrat et al. synthesized neodymium oxide nanorods through thermal decomposition, employing $Nd(OH)_3$ as the precursor and subjecting it to calcination at 550 °C for 2 h [5]. The investigation undertaken by Phuruangrat encompassed the analysis of structure, purified phase, and weight loss characteristics of the synthesized neodymium oxide, utilizing XRD, SEM, TEM, HRTEM, SAED, and TGA. Thermogravimetric analysis (TGA) revealed that the weight loss of the $Nd(OH)_3$ precursor occurred in three distinct stages. Weight loss within the temperature range of 50–270 °C, 270–430 °C and 430–650 °C was attributed to the decomposition of adsorbed residual water on the surface of $Nd(OH)_3$, dehydration of $Nd(OH)_3$ leading to NdOOH formation, and further dehydration of NdOOH into a hexagonal Nd_2O_3 structure, respectively. Various phases of Nd_2O_3 were investigated through XRD analysis. The XRD results indicated that an escalation in calcination temperature induced heightened atomic diffusion. SEM observations elucidated that both the average particle size and the degree of crystallinity increased with the elevation of calcination temperature. Consequently, it can be inferred that calcination temperature significantly influences the average particle size and crystallinity of the product. TEM findings revealed that when $Nd(OH)_3$ was calcined at 450 or 500 °C, the morphology of the resulting neodymium oxide largely consistent. However, when subjected to calcination at 550 °C for 2 h, the product transformed into nanoparticles with an average size of 100 nm.

2.3. Co-precipitation

Zinatloo-Ajabshir et al. employed triethylenetetramine as an innovative precipitant, and $Ho(NO_3)_3 \cdot 6H_2O$ as a precursor for holmium, in order to synthesize nanostructures of holmium oxide through a precipitation method. They also investigated the impact of various capping agents on the morphology and size of the resulting holmium oxide nanoparticles [14]. In this study, Schiff base compound, SDBS, and CTAB were utilized as capping agents. The result of FESEM images demonstrated that CTAB is the most desirable capping agent for the preparation of homogeneous spherical holmium oxide nanoparticles with small grain size. Furthermore, an experiment was conducted to synthesize holmium oxide without the Schiff base compound. FESEM results revealed that in the absence of a capping agent, irregular nano bundles and less uniformly shaped sphere-like nanostructures with large grain sizes were produced. The TEM images indicated that the size of the holmium oxide sample, synthesized using triethylenetetramine and CTAB, fell within the range of 18–60 nm. Zhu et al. synthesized Ho_2O_3 nanostructures employing a multi-step precipitation method. The nanoparticle structures were characterized through TEM, XRD, and XPS analyses. In this investigation, three distinct series of solutions were initially prepared; subsequently, the contents of these solutions were amalgamated, leading to the formation of a yellow precipitate. To enhance clarity, the resultant mixture underwent stirring for duration of 3–4 h (A). Conversely, the combination of holmium (III) oxide and sulfuric acid was subjected to mixing and stirring, followed by gradual addition of deionized water. Upon elevating the temperature to 100°, the outcome was a transparent pink solution (B). The ultimate step in the Ho_2O_3 synthesis process involved merging the mixture of the three primary solutions (A) with the solution obtained from step (B). This amalgamation was stirred for duration of 2 h and subsequently subjected to centrifugation to obtain the desired Ho_2O_3. Remarkably, the holmium oxide synthesized under an excitation wavelength of 785 nm exhibited near-infrared fluorescence within the range of 800–1100 nm [47]. R. Michel et al. employed a solution-coprecipitation method to prepare microsphere nanostructured Nd_2O_3 [37]. Initially, a solution containing $Nd(NO_3)_3 \cdot 6H_2O$ and formic acid was prepared. Upon exposure to an environment with a temperature of 26 °C, the emergence of smoke (NO_2) led to the formation of a white precipitate of neodymium formate. Subsequently, a microwave oven was utilized to facilitate solvent evaporation. Following this, neodymium formate was subjected to calcination within the temperature range of 170 °C to 600 °C under atmospheric conditions, resulting in the formation of single-phase Nd_2O_3 possessing a cubic crystal structure. XRD patterns were obtained at various calcination temperatures. The XRD results revealed that the diffraction peak observed at different calcination temperatures (170, 300, 400, 500, and 600 °C) corresponded to neodymium formate, the decomposition of neodymium formate, the initial crystallization of Nd_2O_3, the cubic phase of Nd_2O_3 and the single-phase cubic structure of Nd_2O_3, respectively. SEM results from samples subjected to evaporation at 70 °C and 170 °C indicated that the particle morphology remained consistent regardless of the evaporation method. Upon calcination at 400 °C, 500 °C, and 600 °C, the SEM images displayed particles with polyhedral shapes that were well-dispersed, nanoparticles of smaller sizes, and spherical shapes with larger pores, respectively. The presence of larger pores at 600 °C compared to 500 °C showed nanoparticle coalescence. ATEM image of the sample calcined at 600 °C demonstrated that the Nd_2O_3 microspheres exhibited low density, discernible by lighter spots within the microspheres.

In another study, Zhaorigetu et al. utilized the precipitation method to synthesize Nd_2O_3 nanoparticles [48]. This particular study employed ammonium tartrate [$(NH_4)2C_4H_4O_6$], neodymium nitrite and distilled water as the initial materials. Zhaorigetu's research delved into the structural and morphological characteristics of the nanoparticles through

techniques such as FT-IR, XRD, SEM, and TEM. The XRD patterns of the neodymium oxides were generated by subjecting the complex to calcination at different temperatures. The results illustrated that at heat treatments of 600, 700, and 800 °C, the structural phase of Nd_2O_3 leads to a pure cubic phase, a combination of cubic (major phase) and hexagonal (minor phase), and well-crystallized hexagonal phase, respectively. TEM images provided insights into the monocrystalline structure of the Nd_2O_3 powders, which exhibited particle sizes within the range of 15–20 nm, with an average size of 18 nm. High-resolution TEM (HRTEM) images revealed a lattice spacing of 0.341 nm.

In another investigation, Huang et al. reported the synthesis of Nd_2O_3 nano-powders using ionic liquid surfactant templates [4]. Huang's investigation focused on the influence of surfactant type and concentration on the precipitation process. The study involved the utilization of N-(3-Cocoamidopropyl)-betaine (CAPB), 1-octyl-3-methylimidazolium chloride ([C_8mim]Cl), and 1-tetradecyl-3-methylimidazolium chloride ([C_{14}mim]Cl) ionic liquid (IL) as surfactant and ammonium hydrogen carbonate (NH_4HCO_3) as precipitant. Conducting concentration tension measurements on ILs, it was determined that the zwitterion surfactant CAPB exhibited lower interfacial tension compared to the cationic surfactants. Consequently, due to CAPB's tendency to form micelles at lower concentrations, it was selected as the surfactant for subsequent investigations The SEM results indicated that the morphology of nanoparticles varied with different concentrations of CAPB. This study encompassed an exploration of the morphology, crystallite size, and particle size of Nd_2O_3 synthesized using varying concentrations of the CAPB surfactant. SEM micrographs of Nd_2O_3 revealed that the microstructures of all the resultant products bore similarities to their precursors. However, those products subjected to calcination at 900 °C exhibited superior uniformity and improved dispersity compared to their precursors. The XRD patterns of the generated Nd_2O_3 unveiled a hexagonal phase for all the products. Consequently, it can be inferred that the concentration of the CAPB surfactant primarily impacts the morphology of Nd_2O_3, while the crystalline phase of Nd_2O_3 remains unaffected.

In another study, Trinh et al. fabricated nanostructures of Nd_2O_3 including nanoporous and nanospheres via the precipitation method [3]. Trinh investigated the morphology and structure of the as-synthesized nanomaterial using X-ray spectroscopy, EDAX, FTIR, SEM, TEM, and HRTEM. The SEM images of neodymium oxide nanospheres and neodymium oxide nanoporous revealed high homogeneity and an irregularly sponge-like structure, respectively. TEM images of Nd_2O_3 nanospheres and Nd_2O_3 nanoporous showed that the particle size of nanomaterials in both cases was approximately 10 nm. The elemental components (wt.%) of Nd_2O_3 nanospheres and Nd_2O_3 nanoporous structures were investigated using EDAX. The presence of carbon (C) has been attributed to oleic acid molecules, which act as capping agent on the spherical particles. Based on XRD results, the diffraction lines of Nd_2O_3 nanospheres were weaker than those of Nd_2O_3 nanoporous structures, suggesting that the spherical particles were coated by amorphous capping agents.

In a separate study, Pingping et al. synthesized Nd_2O_3 nanorods using the precipitation method [49]. Sodium dodecyl benzene sulfonate (SDBS) micelles were employed as templates in this study. The researchers investigated the crystal structure and morphology of Nd_2O_3 through techniques including XRD, SEM, HRTEM, FT-IR, and fluorescence spectrometry. The EDAX pattern of Nd_2O_3 nanorods showed that carbon (C) and copper (Cu) peaks originated from the Cu grids, indicating the presence of only Nd and O present in the nanorods. XRD pattern of Nd_2O_3 were obtained at different concentrations of SDBS and after calcination at 600 °C and 800 °C. The XRD results indicated that the Nd_2O_3 nanorods synthesized at 600 and 800 °C exhibited a pure hexagonal phase. Moreover, enhanced crystallinity was observed in Nd_2O_3 nanorods when the SDBS concentration was maintained at 50 mmol/L. TEM images were acquired for Nd_2O_3 nanorods fabricated within micelles containing different concentrations of SDBS. According to the TEM observations, concentrations of SDBS lower than 1 mmol/L led to the formation of nanorods with a spherical shape and diameters ranging from 20 to 100 nm. As the SDBS concentration exceeded 1 mmol/L, the rod-like Nd_2O_3 structures elongated and widened. Furthermore, prolonged reaction times resulted in the formation of even longer micro-rods. Analysis of the emission spectrum of Nd_2O_3 nanorods at room temperature indicated their fluorescence properties. The excitation and emission peaks were measured at 236 nm and 407 nm, respectively. Fluorescence studies demonstrated that the intensity of fluorescence emission gradually decreased with increasing SDBS concentration, suggesting that Nd_2O_3 nanorods might exhibit fewer defects at higher SDBS concentrations.

In another investigation, Zinatloo-Ajabshir et al. synthesized Nd_2O_3 nanostructures through a straightforward precipitation method [32]. In this study, neodymium nitrate served as the neodymium source, while triethylenetetramine was utilized as a novel precipitant. The authors investigated the impact of various capping agents on the particle size and morphology of Nd_2O_3 nanostructures. This research group demonstrated that the choice of capping agent significantly influenced the morphology and particle size of the Nd_2O_3 nanostructures. According to the FESEM outcomes, SDBS as a capping agent and triethylenetetramine as a precipitant yielded the most favorable results for synthesizing uniformly spherical Nd_2O_3 nanoparticles with fine dimensions. Transmission electron microscopy (TEM) images of the Nd_2O_3 sample exhibited a particle size ranging from approximately 10 to 40 nm.

2.4. *Sonochemical*

Sonochemical synthesis involves employing the principles of sonochemistry to induce chemical reactions in molecules through the application of intense ultrasound radiation. In the context of the present study, holmium nitrate and diethylenetriamine (dien) were utilized as a novel precipitating combination in the synthesis of Ho_2O_3 nanostructures. This innovative method was first explored by Zinatloo-Ajabshir et al. [25], who introduced variations in the type of capping agents to optimize the shape and grain size of the resulting Ho_2O_3 samples. Schiff base, oleylamine, and PVA were all employed as capping agents in the production of Ho_2O_3. To examine the influence of ultrasound irradiation on the dimensions and morphology of Ho_2O_3, a sample was fabricated

without undergoing sonication. It is well-established that in a sonochemical process, elevating the temperature and pressure within the aqueous environment contributes to the formation of particles with uniform and homogeneous morphology. Notably, in the experiment conducted without sonication, particles displayed high levels of agglomeration, resulting in bulky structures. The findings from FE-SEM images, revealing sizes ranging approximately from 14 to 54 nm, underscore the pivotal role of PVA as a capping agent in achieving homogeneity in Ho_2O_3 nanostructures. XRD analysis unveiled that Ho_2O_3 products prior to the calcination phase exhibited an amorphous nature. Following calcination, distinct diffraction patterns corresponding to cubic holmium oxide emerged, signifying a crystalline structure.

Zinatloo-Ajabshir et al. synthesized Nd_2O_3 nanostructures through a sonochemical process using 2,2-dimethyl-1,3-propanediamine as a novel precipitator in the presence of $Nd(NO_3)_3{\cdot}6H_2O$ [39]. The researchers thoroughly examined the impact of varying capping agents on the size and morphology of these nanostructures, employing techniques such as DRS, XRD, FT-IR, FESEM, TEM, and EDAX. The preparation of Nd_2O_3 structures was carried out under different conditions. The preparation of Nd_2O_3 structures was carried out under diverse conditions. Analyzing the FESEM micrographs of neodymium oxide samples in the presence of Schiff base, Titriplex, and PVP revealed distinct outcomes: irregular plate-like microstructures/non-uniform nanobundles for Schiff base, less uniform micro/nanobundles for Titriplex, and uniform spherical structures for PVP. The utilization of PVP as the capping agent appeared to significantly influence the sonochemical fabrication of uniform spherical Nd_2O_3 nanostructures, exhibiting sizes ranging from 15 to 75 nm. To comprehend the role of ultrasound irradiation on the dimensions and configuration of Nd_2O_3, the reaction was also conducted without sonication. The outcomes from FESEM micrographs underscored that neodymium oxide acquired without sonication displayed irregular microstructures and bulk formations. The schematic diagram of rare earth metal oxide nanostructures is shown in Fig. 4.

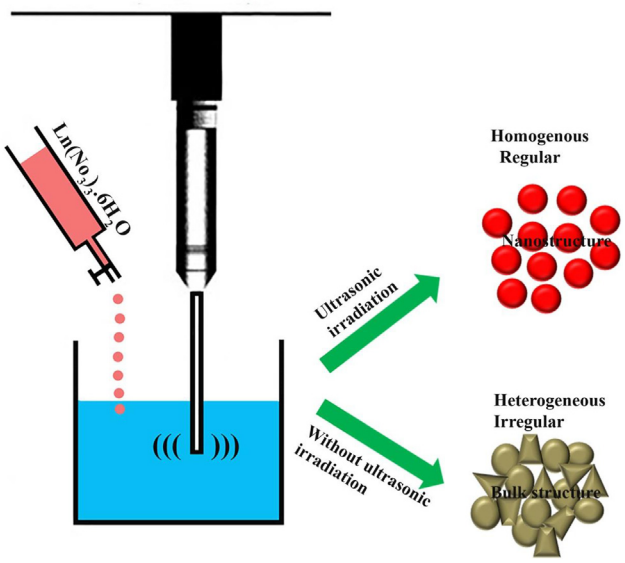

Fig. 4 – Schematic representation of the synthesis of holmium oxide and neodymium oxide using the sonication method.

2.5. *Other preparation approaches for Ho_2O_3 nanostructures*

2.5.1. *Spark plasma sintering (SPS)*

The utilization of the pulse electric current sintering technique, commonly referred to as spark plasma sintering (SPS), presents distinct advantages due to its implementation of lower sintering temperatures and higher heating rates (exceeding 100 °C/min). In comparison with conventional methods like pressureless vacuum sintering and hot isostatic pressing (HIP), SPS offers significantly reduced sintering times, often spanning only several hours. This abbreviated processing time renders the technique particularly advantageous for assessing dopant effects and expanding the material database across various substances. An illustrative instance is evident in the work of Furuse and colleagues, who harnessed the pulse electric current sintering approach to craft transparent Ho_2O_3 ceramics. Notably, their study marked the pioneering exploration of Ho_2O_3 potential as a Faraday rotator within high-average power lasers [19].

In another investigation, Cheng et al. fabricated transparent magneto-optical Ho_2O_3 ceramics using a vacuum sintering approach [21]. In this method, the self-reactive resultant HoOF was employed as a sintering aid. FE-SEM micrographs were captured to depict the surface microstructures of the Ho_2O_3 ceramics that were vacuum-sintered at temperatures ranging from 1400 °C for 0–16 h and from 1350 to 1500 °C with a constant holding time of 4 h. The FE-SEM results demonstrated that the average grain size increased with longer residence time and higher sintering temperature. To identify the optimal molar ratio (R) of F^-/Ho^{3+} and sintering temperature for achieving the desired optical quality in the sintered bodies, the reaction was conducted at different molar ratios and temperatures. The outcomes indicated that the most favorable Ho_2O_3 ceramic sample, exhibiting a relatively uniform thickness of 6–9 nm and an in-line transmittance of 72.0% at 1550 nm, was obtained with an optimal F^-/Ho^{3+} molar ratio of 0.01 and sintering temperature of 1850 °C.

In another investigation, Lu et al. synthesized Ho_2O_3 nanoparticles with a ceramic structure through a precipitation-assisted route consisting of two stages: precipitation and calcination. They then evaluated the magneto-optical characteristics of holmium oxide (Ho_2O_3) ceramics [22]. In this study, Ho_2O_3 ceramics were synthesized using sulfate-exchanged nitrate-type layered rare-earth hydroxide as the precipitation precursor. The ceramics were sintered at a relatively low vacuum temperature of 1700 °C, resulting in an average particle size of ~48 nm and an inline transmittance of ~73 % at 1000 nm. The researchers observed that the calcination temperature for the Ho_2O_3 powder significantly influenced the optical quality of the sintered body. The optimum calcination temperature was found to be 1050 °C.

Hu et al. prepared transparent Ho_2O_3 ceramics through a combination of vacuum pre-sintering and the hot isostatic pressing (HIP) method. Holmium ceramics were synthesized

using calcined commercial Ho_2O_3 powder with high purity as the starting material, heated at 1000 °C for 4 h. Vacuum pre-sintering and HIP were conducted at temperatures of 1250 °C and 1450 °C, respectively, resulting in holmium ceramics with an average size of 0.77 μm and a dense structure. The pre-sintering and HIP processes lasted 2 h and 3 h, respectively. The study's results highlighted the significant impact of sintering temperature on the morphology and relative density of Ho_2O_3 ceramics. Furthermore, the presence of compressed pores in the Ho_2O_3 ceramics was confirmed through an investigation into the effects of air annealing on the optical quality of the ceramics [50].

2.5.2. *Electrochemical deposition*

For the first time, Shiri et al. prepared Ho_2O_3 nanoparticles using the electrosynthesis approach as an environmentally friendly method to create a composite electrode (POAP/Ho_2O_3) for use as a supercapacitor electrode material. Hybrid films consisting of poly ortho aminophenol (POAP) and Ho_2O_3 were generated through potentiodynamic deposition from solutions containing ortho aminophenol and Ho_2O_3. The main objective of this study was to investigate the POAP/Ho_2O_3 composite and its potential to enhance the cycling ability of the electrode. XRD results revealed strong and sharp peaks at $2\theta = 29$ °, 34 °, 48.5 °, and 58°, characteristic of Ho_2O_3. Additionally, EDAX spectrum and SEM image confirmed the successful synthesis of electro-synthesized nanoparticles [26].

2.6. *Other preparation approaches for Nd_2O_3 nanostructures*

2.6.1. *Sol-gel*

The sol-gel process is a wet-chemical technique employed for the fabricating both glassy and ceramic materials. In this method, the sol (or solution) gradually transforms into a gel-like network containing both a liquid phase and a solid phase. Yang et al. utilized an additive agent, polyvinyl alcohol, to fabricate Nd_2O_3 nanopowders through the sol-gel auto-combustion method [31]. This study also encompassed the investigation of XRD, TEM, AFM, and the catalytic esterification activity of the as-prepared Nd_2O_3 nanopowders. Yang and colleagues explored the influence of various factors on the composition and preparation of the particles, including the molar ratio of Nd^{3+} to citric acid, the pH value of the reaction system, and the quantity of the additive factor, polyvinyl alcohol. The optimal conditions were determined to be 10 % polyvinyl alcohol relative to $Nd(NO_3)_3$ and a molar ratio of Nd3+ to citric acid at 1:2. XRD results revealed that an increase in calcination temperature led to a larger grain size for the nanoparticles. TEM analysis demonstrated that increasing the amount of polyvinyl alcohol from 10 % to 20 % resulted in a growth in the grain size of the nanoparticles, which correlated well with the XRD patterns. Ultimately, the synthesis of Nd_2O_3 nanopowders with a particle size of 20–30 nm was achieved under the desirable conditions of a molar ratio of 1: 2 Nd^{3+} to citric acid and 10 % polyvinyl alcohol.

In a separate study, Zawadzki et al. produced neodymium oxide nanoparticles with different morphologies using the sol-gel method combined with solvothermal treatment and simple neodymium salts [40]. To start, they prepared neodymium salts (nitrate or acetate), which were then dissolved using distilled water or alcohol (ethanol, butanol, or methanol). The resulting solution was introduced into an autoclave and heated within the temperature range of 140–220 °C for 4–8 h. The formed gel was separated from the solvent via centrifugation, dried in a vacuum, and subsequently heat-treated at temperatures up to 800 °C. This process eventually led to the formation of neodymium coatings on two different substrates (glass slides and stainless steel plates), achieving a thickness of approximately 5 μm. The XRD patterns of the samples synthesized under hydrothermal conditions (T = 140 °C and T = 160 °C, t = 4 h) using neodymium acetate and neodymium nitrate were examined at various calcination temperatures. The XRD results illustrated that the pure hexagonal phase of neodymium oxide emerged after treatment at temperatures exceeding 500 °C. The average diameter of the as-prepared Nd_2O_3 particles, estimated through TEM, was around 8 nm. TEM images revealed that around and particles began to aggregate at higher temperatures.

2.6.2. *Green synthesis*

Lembang et al. employed a green synthesis approach to produce Nd_2O_3 nanoparticles, utilizing an aqueous extract of *Terminalia catappa* leaves (TLE) as a source of weak base and $Nd(NO_3)_3$ as a precursor [38]. They created a mixed solution containing $Nd(NO_3)_3$ and TLE in a 5:1 ratio. This mixture was stirred at 50 °C for 1 h, leading to the formation of a sol and subsequently a gel. The formed gel underwent drying and calcination at 600 °C for 2 h. The resultant neodymium oxide powder exhibited a violet color and had particle sizes ranging from 40 to 60 nm. The functional groups present in TLE, such as alkaloids and saponins, played crucial roles in the synthesis of Nd_2O_3 nanoparticles.

2.6.3. *Combustion*

Umesh et al. prepared nanocrystalline Nd_2O_3 phosphors with a spherical structure using the combustion method. Umesh investigated PXRD, SEM, TEM, and Raman spectra, as well as the photoluminescence spectrum of the as-prepared Nd_2O_3 phosphors [28]. The PXRD result of the as-formed Nd_2O_3 combustion product revealed an amorphous Nd_2O_3 phase along with neodymium oxide carbonate ($Nd_2O_2CO_3$) peaks. After calcination at 900 °C for 3 h, the PXRD pattern transformed into the hexagonal phase with A-type Nd_2O_3. The SEM micrograph demonstrated that the shape of Nd_2O_3 was agglomerated, foamy, crispy, and porous. However, after calcination at 900 °C for 3 h, the shape of the particles became spherical with smooth surfaces. Nd_2O_3 powders with spherical structures had particle sizes in the range of 20–100 nm.

2.6.4. *Radiofrequency (RF) thermal plasma route*

Due to its single-step preparation process and direct route through vapor phase nucleation and plasma evaporation, the method is particularly interesting and suitable for high-melting-point refractory materials like Nd_2O_3, leading to the synthesis hexagonal phase. The thermal plasma preparation of nanopowders via evaporation, quenching, and nucleation utilizing arc plasma sources or radio frequency (RF) is a well-definite technique for the mass production of new

nanomaterials [34]. RF thermal plasma sources at atmospheric pressure are gaining importance in the production of high-purity nanomaterials for various high-end technological applications. Dhamale et al. fabricated Nd_2O_3 nanoparticles using an inductively coupled radiofrequency thermal plasma route [34]. In their study, the atmospheric pressure RF thermal plasma reactor exhibited high temperature together and a sharp temperature gradient. Micron-sized Nd_2O_3 powder, ranging in sizes from 1 to 25 μm, was used as a precursor for the synthesis of Nd_2O_3 nanocrystal. The carrier gas, loaded with micron-size Nd_2O_3 powder, was introduced at the center of the plasma plume, resulting in the formation of supersaturated vapor. As the vapor moved downstream, nucleation and growth of Nd_2O_3 particles occurred due to the steep temperature gradient. Upon reaching a certain temperature downstream, nucleation ceased, and the particles attained their final nanometer-scale size. These particles were then deposited on the inner wall of the plasma torch. The deposited nanoparticles were collected, analyzed for phase formation, crystallinity, size distribution, and other characteristics. XRD spectra of the raw precursor and nanocrystalline of Nd_2O_3 were acquired and compared with standard spectra. Comparison revealed that the precursor particles possessed the crystal structure of neodymium hydroxide, whereas the synthesized nanocrystalline Nd_2O_3 exhibited the hexagonal phase of the Nd_2O_3 crystal structure. The XRD results also indicated that Nd_2O_3 nanoparticles required heat treatment at temperatures exceeding 900 °C to transition from the cubic to the hexagonal phase. SEM micrographs showed that the size of precursor powder particles from 1 to 25 μm, while the size of synthesized nanoparticles was less than 100 nm. TEM image of the synthesized Nd_2O_3 nanoparticles demonstrated uniformity in size and shape.

2.6.5. *Hydrogen plasma-metal reaction (HPMR) method*

The HPMR technique is a novel vapor deposition process that is appropriate for industrially producing ultrafine particles (UFPs) of various metals at a low cost and with high purity. The driving force for particles production via HPMR was found to be closely dependent on factors such as the melting points of metals, the evaporation heat of metals, and the heat of formation for recombination from atoms to molecules of hydrogen [51–53]. Liu et al. succeeded in directly synthesizing neodymium oxide nanoparticles using the HPMR method without the need for oxidation [6]. In fact, Nd hydride nanoparticles were first prepared via the hydrogen plasma-metal reaction (HPMR) method. Subsequently, Nd oxide nanostructures were synthesized directly from the passivation of Nd hydride nanoparticles. The XRD pattern results demonstrated that the Nd hydride nanoparticles underwent oxidation even during the passivation process, resulting in the production of very pure Nd_2O_3 with a cubic structure instead of the hydride. TEM image revealed that the passivated nanoparticles of Nd_2O_3 were almost spherical in shape, with particle sizes in the range of 5–50 nm.

2.6.6. *Inverse microemulsion technique*

A reverse microemulsion is defined as a thermodynamically stable, isotropic dispersion of an aqueous phase within a continuous oil phase, stabilized by an interfacial layer of surfactant molecules. Reverse micelles that exist in a microemulsion system, essentially nanometer-aqueous droplets with specific compositions, are recognized for providing an excellent medium for synthesizing nanoparticles with uniform morphologies and exceptional homogeneity [54]. Que et al. employed the inverse microemulsion technique to fabricate neodymium oxide nanocrystals [41]. XRD spectrum and TEM analysis demonstrated that the neodymium oxide nanoparticles exhibited a nanocrystalline structure, with varying sizes ranging from 5 to 60 nm, respectively.

2.6.7. *Microwave irradiation (MWI)*

MWI techniques, offering rapid and convenient pathways for nanostructuring, possess a unique capability for large-scale preparation without being susceptible to thermal gradient effects. This method enables the acceleration of reactions through microwave technology, presenting an opportunity to regulate the particle size and morphology of nanostructures, ranging from small spherical nuclei to short rods, and even extended assemblies of nanowires. Panda et al. synthesized Nd_2O_3 nanorods and investigated the manipulation of the particle size and morphology in rare earth oxide (M_2O_3, M = Pr, Nd, Sm, Eu, Gd, Tb, Dy) by altering the relative concentrations of the organic surfactants and MWI reaction time [36].

3. Conclusion

In this review, we have thoroughly examined the synthesis methods and morphological control of Holmium Oxide (Ho_2O_3) and Neodymium Oxide (Nd_2O_3) nanoparticles. These two compounds, belonging to the rare earth element family, play pivotal roles in various industries, including optics, magnetism, and catalysis. Our study has unveiled significant insights into the influence of synthesis parameters on the size, morphology, and properties of these nanoparticles. Notably, the hydrothermal method has proven to be an effective choice for Ho_2O_3 synthesis due to its precise control over temperature, time, and pH. Additionally, the Spark Plasma Sintering (SPS) method has been optimized for producing transparent optical magnetic Ho_2O_3 ceramics. For the synthesis of Nd_2O_3, we have explored several methods, each offering distinct advantages. The sol-gel technique, for instance, provides the benefit of obtaining smaller-sized nanoparticles. Furthermore, radio frequency (RF) thermal plasma methods, high-pressure microwave routes, and microwave radiation methods have shown promise for large-scale production of economically viable and highly pure Nd_2O_3 nanoparticles. In summary, our research highlights the direct impact of the synthesis method on the shape and distribution of Ho_2O_3 and Nd_2O_3 nanostructures. These findings offer valuable guidance for the design and production of new rare earth oxides tailored to specific industrial applications.

Declaration of competing interest

The authors declare that they have no known competing financial interests or personal relationships that could have appeared to influence the work reported in this paper.

REFERENCES

[1] Hossain MK, Khan MI, El-Denglawey A. A review on biomedical applications, prospects, and challenges of rare earth oxides. Appl Mater Today 2021;24:101104.

[2] Hossain MK, Ahmed MH, Khan MI, Miah MS, Hossain S. Recent progress of rare earth oxides for sensor, detector, and electronic device applications: a review. ACS Appl Electron Mater 2021;3:4255–83.

[3] Trinh LH, Khieu DQ, Thai Long H, Thai Hoa T, Tuan Quang D, Duc Cuong N. A novel approach for synthesis of hierarchical mesoporous Nd2O3 nanomaterials. J Rare Earths 2017;35:677–82.

[4] Huang B, Huang C, Chen J, Sun X. Size-controlled synthesis and morphology evolution of Nd2O3 nano-powders using ionic liquid surfactant templates. J Alloys Compd 2017;712:164–71.

[5] Phuruangrat A, Thongtem S, Thongtem T. Template-free synthesis of neodymium hydroxide nanorods by microwave-assisted hydrothermal process, and of neodymium oxide nanorods by thermal decomposition. Ceram Int 2012;38:4075–9.

[6] Liu T, Zhang, Shao Li. Synthesis and characteristics of Sm2O3 and Nd2O3 nanoparticles. Langmuir 2003;19:7569–72.

[7] Pourmortazavi SM, Rahimi-Nasrabadi M, Aghazadeh M, Ganjali MR, Karimi MS, Norouzi P. Synthesis, characterization and photocatalytic activity of neodymium carbonate and neodymium oxide nanoparticles. J Mol Struct 2017;1150:411–8.

[8] Barbora L, Singh R, Shroti N, Verma A. Synthesis and characterization of neodymium oxide modified nafion membrane for direct alcohol fuel cells. Mater Chem Phys 2010;122:211–6.

[9] Lee HI, Lee SW, Rhee CK, Sohn Y. Paramagnetic Ho2O3 nanowires, nano-square sheets, and nanoplates. Ceram Int 2018;44:17919–24.

[10] Mortazavi-Derazkola S, Zinatloo-Ajabshir S, Salavati-Niasari M. Novel simple solvent-less preparation, characterization and degradation of the cationic dye over holmium oxide ceramic nanostructures. Ceram Int 2015;41:9593–601.

[11] Zinatloo-Ajabshir S, Salavati-Niasari M, Sobhani A, Zinatloo-Ajabshir Z. Rare earth zirconate nanostructures: recent development on preparation and photocatalytic applications. J Alloys Compd 2018;767:1164–85.

[12] Shirzadi-Ahodashti M, Ebrahimzadeh MA, Amiri O, Naghizadeh A, Mortazavi-Derazkola S. Novel NiFe/Si/Au magnetic nanocatalyst: biogenic synthesis, efficient and reusable catalyst with enhanced visible light photocatalytic degradation and antibacterial activity. Appl Organomet Chem 2020;34:e5467.

[13] Mortazavi-Derazkola S, Zinatloo-Ajabshir S, Salavati-Niasari M. Facile hydrothermal and novel preparation of nanostructured Ho2O3 for photodegradation of eriochrome black T dye as water pollutant. Adv Powder Technol 2017;28:747–54.

[14] Zinatloo-Ajabshir S, Mortazavi-Derazkola S, Salavati-Niasari M. Preparation, characterization and photocatalytic degradation of methyl violet pollutant of holmium oxide nanostructures prepared through a facile precipitation method. J Mol Liq 2017;231:306–13.

[15] Kim J, Luo ZX, Wu Y, Lu X, Jay M. In-situ formation of holmium oxide in pores of mesoporous carbon nanoparticles as substrates for neutron-activatable radiotherapeutics. Carbon 2017;117:92–9.

[16] Vasyliev V, Villora EG, Nakamura M, Sugahara Y, Shimamura K. UV-visible Faraday rotators based on rare-earth fluoride single crystals: LiREF4 (RE = Tb, Dy, Ho, Er and Yb), PrF3 and CeF3. Opt Express 2012;20:14460–70.

[17] Zheleznov D, Starobor A, Palashov O, Lin H, Zhou S. Improving characteristics of Faraday isolators based on TAG ceramics by cerium doping. Opt Lett 2014;39:2183–6.

[18] Yasuhara R, Tokita S, Kawanaka J, Kawashima T, Kan H, Yagi H, et al. Cryogenic temperature characteristics of Verdet constant on terbium gallium garnet ceramics. Opt Express 2007;15:11255–61.

[19] Morales JR, Amos N, Khizroev S, Garay JE. Magneto-optical Faraday effect in nanocrystalline oxides. J Appl Phys 2011;109.

[20] Furuse H, Yasuhara R. Magneto-optical characteristics of holmium oxide (Ho2O3) ceramics. Opt Mater Express 2017;7:827–33.

[21] Cheng H, Lu B, Liu Y, Zhao Y, Sakka Y, Li J-G. Transparent magneto-optical Ho2O3 ceramics: role of self-reactive resultant oxyfluoride additive and investigation of vacuum sintering kinetics. Ceram Int 2019;45:14761–7.

[22] Lu B, Cheng H, Xu X, Chen H. Preparation and characterization of transparent magneto-optical Ho2O3 ceramics. J Am Ceram Soc 2019;102:118–22.

[23] Guo C, Dong X, Zhang X, Cheng X, Li Q, Sun Y, et al. Controllable construction of Ho2O3 nanomaterials with different dimensions (1D, 2D, and 3D) for real-time monitoring human breathing and body surface humidity detection. J Mater Chem A 2021;9:11632–40.

[24] Abdusalyamova MN, Makhmudov FA, Shairmardanov EN, Kovalev ID, Fursikov PV, Khodos II, et al. Structural features of nanocrystalline holmium oxide prepared by the thermal decomposition of organic precursors. J Alloys Compd 2014;601:31–7.

[25] Zinatloo-Ajabshir S, Mortazavi-Derazkola S, Salavati-Niasari M. Sono-synthesis and characterization of Ho2O3 nanostructures via a new precipitation way for photocatalytic degradation improvement of erythrosine. Int J Hydrogen Energy 2017;42:15178–88.

[26] Shiri HM, Ehsani A. A novel and facile route for the electrosynthesis of Ho2O3 nanoparticles and its nanocomposite with p-type conductive polymer: characterisation and electrochemical performance. Bull Chem Soc Jpn 2016;89:1201–6.

[27] Mortazavi-Derazkola S, Zinatloo-Ajabshir S, Salavati-Niasari M. New sodium dodecyl sulfate-assisted preparation of Nd2O3 nanostructures via a simple route. RSC Adv 2015;5:56666–76.

[28] Umesh B, Eraiah B, Nagabhushana H, Nagabhushana BM, Nagaraja G, Shivakumara C, et al. Synthesis and characterization of spherical and rod like nanocrystalline Nd2O3 phosphors. J Alloys Compd 2011;509:1146–51.

[29] Biswas S, Naskar H, Pradhan S, Wang Y, Bandyopadhyay R, Pramanik P. Simultaneous voltammetric determination of Adrenaline and Tyrosine in real samples by neodymium oxide nanoparticles grafted graphene. Talanta 2020;206:120176.

[30] Al-Fakeh MS, Al-Otaibi NF. Nd_2O_3, Cr_2O_3, and V_2O_3 nanoparticles via calcination: synthesis, characterization, antimicrobial and antioxidant activities. J Nanotechnol 2022;2022:7794939.

[31] Yang W, Qi Y, Ma Y, Li X, Guo X, Gao J, et al. Synthesis of Nd2O3 nanopowders by sol–gel auto-combustion and their catalytic esterification activity. Mater Chem Phys 2004;84:52–7.

[32] Zinatloo-Ajabshir S, Mortazavi-Derazkola S, Salavati-Niasari M. Nd2O3 nanostructures: simple synthesis, characterization and its photocatalytic degradation of methylene blue. J Mol Liq 2017;234:430–6.

[33] Zinatloo-Ajabshir S, Mortazavi-Derazkola S, Salavati-Niasari M. Schiff-base hydrothermal synthesis and characterization of Nd2O3 nanostructures for effective

photocatalytic degradation of eriochrome black T dye as water contaminant. J Mater Sci Mater Electron 2017;28:17849–59.
[34] Dhamale GD, Mathe VL, Bhoraskar SV, Sahasrabudhe SN, Ghorui S. Synthesis and characterization of Nd2O3 nanoparticles in a radiofrequency thermal plasma reactor. Nanotechnology 2016;27:085603.
[35] Kubra KT, Sharif R, Patil B, Javaid A, Shahzadi S, Salman A, et al. Hydrothermal synthesis of neodymium oxide nanoparticles and its nanocomposites with manganese oxide as electrode materials for supercapacitor application. J Alloys Compd 2020;815:152104.
[36] Panda AB, Glaspell G, El-Shall MS. Microwave synthesis and optical properties of uniform nanorods and nanoplates of rare earth oxides. J Phys Chem C 2007;111:1861–4.
[37] Michel CR, Martínez-Preciado AH, Contreras NLL. Gas sensing properties of Nd2O3 nanostructured microspheres. Sensor Actuator B Chem 2013;184:8–14.
[38] Lembang MS, Yulizar Y, Sudirman S, Apriandanu DOB. A facile method for green synthesis of Nd2O3 nanoparticles using aqueous extract of Terminalia catappa leaf. AIP Conf Proc 2018:2023.
[39] Zinatloo-Ajabshir S, Mortazavi-Derazkola S, Salavati-Niasari M. Sonochemical synthesis, characterization and photodegradation of organic pollutant over Nd2O3 nanostructures prepared via a new simple route. Separ Purif Technol 2017;178:138–46.
[40] Zawadzki M, Kępiński L. Synthesis and characterization of neodymium oxide nanoparticles. J Alloys Compd 2004;380:255–9.
[41] Que W, Kam CH, Zhou Y, Lam YL, Chan YC. Yellow-to-violet upconversion in neodymium oxide nanocrystal/titania/ormosil composite sol–gel thin films derived at low temperature. J Appl Phys 2001;90:4865–7.
[42] Gan YX, Jayatissa AH, Yu Z, Chen X, Li M. Hydrothermal synthesis of nanomaterials. J Nanomater 2020;2020:8917013.
[43] Yang G, Park SJ. Conventional and microwave hydrothermal synthesis and application of functional materials: a review. Materials 2019:12. Basel, Switzerland).
[44] Jeon SH, Nam K, Yoon HJ, Kim Y-I, Cho DW, Sohn Y. Hydrothermal synthesis of Nd2O3 nanorods. Ceram Int 2017;43:1193–9.
[45] Kępiński L, Zawadzki M, Miśta W. Hydrothermal synthesis of precursors of neodymium oxide nanoparticles. Solid State Sci 2004;6:1327–36.
[46] Mortazavi-Derazkola S, Zinatloo-Ajabshir S, Salavati-Niasari M. Preparation and characterization of Nd2O3 nanostructures via a new facile solvent-less route. J Mater Sci Mater Electron 2015;26:5658–67.
[47] Zhu J, Shao XJ, Li Z, Lin CH, Wang CW, Jiao K, et al. Synthesis of holmium-oxide nanoparticles for near-infrared imaging and dye-photodegradation27; 2022. Molecules (Basel, Switzerland).
[48] Zhaorigetu B, Ridi G, Min L. Preparation of Nd2O3 nanoparticles by tartrate route. J Alloys Compd 2007;427:235–7.
[49] Wu P, Zhang Z, Song G. Preparation of Nd2O3 nanorods in SDBS micelle system. J Rare Earths 2014;32:1027–31.
[50] Hu D, Li X, Snetkov I, Yakovlev A, Balabanov S, Ivanov M, et al. Fabrication, microstructure and optical characterizations of holmium oxide (Ho2O3) transparent ceramics. J Eur Ceram Soc 2021;41:759–67.
[51] Liu T, Zhang T, Qin C, Zhu M, Li X. Improved hydrogen storage properties of Mg–V nanoparticles prepared by hydrogen plasma–metal reaction. J Power Sources 2011;196:9599–604.
[52] Liu T, Shao H, Li X. Synthesis of Fe–Al nanoparticles by hydrogen plasma–metal reaction. J Phys Condens Matter 2003;15:2507.
[53] Li JY, Mei QS. Synthesis of nanoparticles of titanium aluminides by hydrogen plasma–metal reaction: effects of master alloy composition and chamber pressure on particle size, composition and phase. Powder Metall 2015;58:209–13.
[54] Xu P, Han X, Wang M. Synthesis and magnetic properties of BaFe12O19 hexaferrite nanoparticles by a reverse microemulsion technique. J Phys Chem C 2007;111:5866–70.
[55] Tabanli S, Bilir G, Eryurek G. Optical properties and Judd–Ofelt analysis of Nd2O3 nanocrystals embedded in polymethyl methacrylate. J Rare Earths 2018;36:170–8.

Mina Shirzadi-Ahodashti: Assistant professor at Mazandaran University of medical sciences, Iran.

Sobhan Mortazavi-Derazkola: Assistant professor at Birjand University of medical sciences, Iran.

Mohammad Ali Ebrahimzadeh: Professor at Mazandaran University of medical sciences, Iran.